30th Congress of the International Council of the Aeronautical Sciences
DCC, Daejeon, Korea ; September 25-30, 2016

INVESTIGATION ON OBLIQUE SHOCK WAVE CONTROL BY SURFACE ARC DISCHARGE PLASMA

F Liu*, H Yan, J Xu***
*** Northwestern Polytechnical University, China,**
****Northwestern Polytechnical University, China,**
****Collaborative Innovation Center for Advanced Aero-Engine, China**

Keywords: *surface arc discharge, flow control, oblique shock, experiment and simulation*

Abstract

The mechanism of oblique shock wave control by surface arc discharge plasma is explored through a combined numerical and experimental study. The experiments are conducted in a Mach 2.5 supersonic tunnel with static pressure of 0.3bar and temperature of 130K. An oblique shock is formed by a compression ramp with the angle of 7 °mounted on the lower wall of the wind tunnel. Six electrodes are arranged equally spaced in the spanwise direction and upstream of the oblique shock. Two types of discharge are observed. One is generated between the two adjacent electrodes, forming a transversal arc. While the other one is formed between the electrode and the compression ramp due to high power input, thus a streamwise arc is observed. It is found that the streamwise arc is relatively stable compared to the transversal one, therefore is chosen in this study. The experimental results show that the presence of the stable arc discharge effectively reduces the oblique shock strength, leading to the increase of shock angle which is measured by Schlieren technique. A three-dimensional numerical simulation is performed and the surface arc discharge plasma is modeled as an equivalent heating source based on the thermal effect of plasma. Results show that the surface pressure increases in front of the oblique shock and decreases behind the shock, which is in good agreement with the experimental measurement. This validates the assumption of the arc discharge plasma model, and further confirms the predominant role of the thermal effect of plasma played in the shock manipulation.

1 Introduction

Flow control based on the plasma actuation is a novel technique to improve the aerodynamic characteristics and propulsion efficiency of aircraft. In the investigation of the plasma active flow control, many types of plasma actuations are developed such as Surface Corona Discharge actuator [1], Surface Dielectric Barrier Discharge (DBD) actuator [2], Localized Arc Filament Plasma actuator [3, 4] and Plasma Synthetic Jet actuator [5], which have many advantageous features including inertialess, exibility, simplicity, low power consumption and ability for real-time control at high frequency [6]. So in recent years plasma flow control has drawn considerable attention and been widely applied in boundary layer acceleration to control laminar-turbulent transition [7], airfoil separation control [8], high speed jet control [9, 10] and shock wave control in supersonic inlet [11, 12].

The mechanism for plasma flow control can be summarized as aerodynamic effect, thermal effect and chemical effect [13]. A maximal velocity of 10m/s can be induced by DBD actuator [14] in the near-surface region due to the aerodynamic effect, which can be applied in laminar-turbulent transition control; Thermal effect induces local gas pressure and temperature rise in the arc region which modifies the high speed flow effectively; Chemical effect adds new particles, such as ions, electrons and excited particles into flow field which change the gas properties. The last two effects are more attractive in shock wave control by arc discharge plasma. Wang et al. [15] theoretically analyzed the last two effects on the

shock wave using a thermal choking model and an ionic sound wave model and verified the dominant role of the thermal effect by experiments. In the experimental study by Leonov et al. [16, 17], it was found the extrusive layer excited by the transversal quasi-dc surface discharge leaded to the upstream shifting of oblique shock and increasing of the shock angle. More importantly it revealed that the slow vibrational-translational (V-T) relaxation in air could expand the extrusive layer downstream significantly so as to modify the flow more effectively. The transversal electrical discharge laments with a typical gas temperature of about 3000 K oscillated greatly at about 10-30 kHz. In their experiments with high power (3-17kW) applied to the discharge [18], the plasma generation accompanied by the formation of a new oblique shock, which weakened the original oblique shock downstream. Despite of an unstable behavior of the transversal discharge the position of the induced shock was stable, predictable, and allowed regulation by means of discharge parameters. Alexander et al. [11] studied a mid-scale model inlet response to unsteady and non-uniform plasma generation in the immediate vicinity of the ramp. It was shown that two-shock wave structure was transformed to single-shock configuration with consequent artificial soft curved surface of isentropic compression. In the off-design mode the plasma generation caused increase of mass flow rate at moderate power deposition. In most cases the plasma deposition leaded to the increase of pressure recovery coefficient due to the reduction of pressure loss and replacement of shock waves with a series of isentropic compression waves.

Most of the research studied the plasma flow control using high discharge power, which could induce strong shock waves to perturb the flow field. Therefore, the effect of the newly generated shock waves and the thermal effect of plasma are intertwined in most applications of plasma control. This paper is only focused on exploring the thermal effect of plasma on the oblique shock wave. A small discharge power of 600-900Walts is applied to avoid the generation of strong shock waves. Both experiment and simulation are performed to elaborate on the control mechanism of thermal effect.

2 Experimental Facility

The experiments are conducted in a small-scale short-duration supersonic wind tunnel with design Mach number of 2.5 as shown in Fig.1. The incoming flow in the test section with height of 75mm and width of 40mm has initial Mach number of 2.5, static pressure p=0.17-0.32bar and temperature T=130K. An oblique shock is generated by a ramp whose angle is 7 ° with height of 3mm. The electrode row includes 6 tungsten tabs of 2mm in diameter arranged by sequence of null-cathode-anode-anode-cathode-null with 2mm equally spaced in the spanwise direction as shown schematically in Fig.2. All electrodes are flush-mounted in ceramic and 32mm upstream of the ramp. Fig.3 depicts the experimental circuit. The power supply consists of a high-voltage DC circuit and a resistor box. The maximal output voltage and current of the DC circuit can reach up to 10 kV and 1A, respectively. Such high voltage is used for electrical breakdown of the air. The resistor box consists of 16 resistors with 10kΩ and 1kW each and is used to restrict and stabilize the current after the air is broken down. Four pressure sensors labeled as P1, P2, P3 and P4 are used to record the pressure change between the discharge on and off. Their locations are shown in Fig.4. The Schlieren images of the oblique shock are collected to measure the shock angle. The voltage and current of discharge arc are monitored by a voltage probe and a current probe with a signal amplifier, respectively.

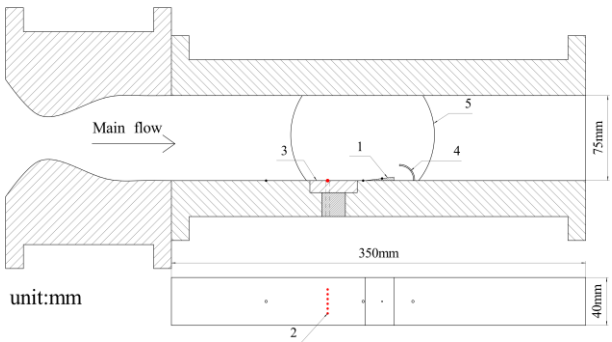

Fig.1 Schematic of Wind Tunnel Setup (1-ramp, 2-electrode row, 3-ceramic, 4-Pitot tube, 5-Schlieren window)

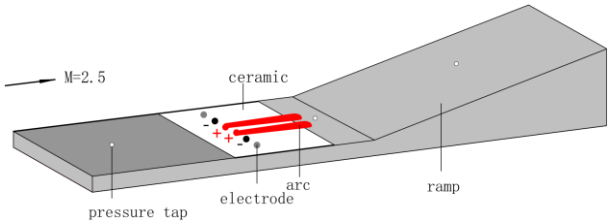

Fig.2 Schematic of Arc Discharge

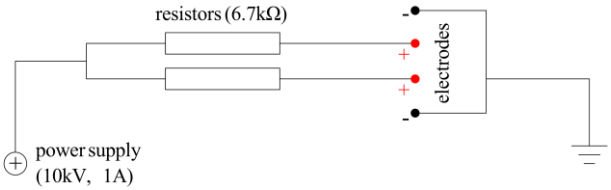

Fig.3 Experimental Circuit

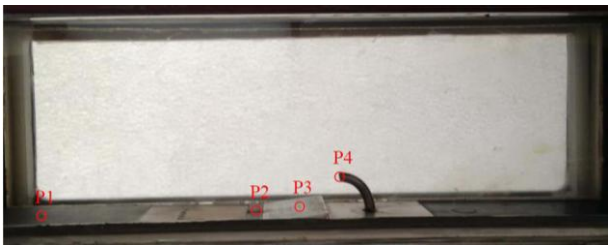

(a) Pressure Tab Location

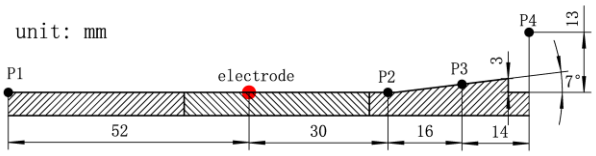

(b) Specific Streamwise Location of Pressure Tab

Fig.4 Pressure Tab Layout

3 Numerical Method

The three-dimensional ideal compressible flow governing equations are written as:

$$\frac{\partial \rho}{\partial t} + \nabla \cdot (\rho U) = 0 \qquad (1)$$

$$\frac{\partial (\rho U)}{\partial t} + \nabla \cdot (\rho U U) = -\nabla p + \nabla \cdot \tau \qquad (2)$$

$$\frac{\partial (\rho h)}{\partial t} + \nabla \cdot [(\rho h + p) U] = \nabla \cdot (\lambda \nabla T) + \Phi + S \qquad (3)$$

where τ is the stress tensor, Φ is the viscous work term and S is the user defined heat source which stands for the plasma heating in this study. A 3D flow field extracted from the experiment is simulated based on the steady density-based solver of FLUENT. The third-order accurate AUSM scheme is adopted for convective flux terms. The second-order upwind scheme is used for spatial discretization of variables. The standard k-ε turbulence model is utilized. Based on the thermal effect of plasma, the arc discharge is modeled as a steady heating source with equivalent discharge power, which will be introduced in detail in the following section.

The whole computational domain is shown in Fig.5. The incoming flow is Mach 2.5 with static pressure of 0.3bar and temperature of 130K. The first-order extrapolation is used for the outlet. No-slip and adiabatic conditions are specified on the upper, lower and side walls. The symmetry condition is used for the symmetric plane. Considering the protruding of the electrode row, it is simplified as a rectangular with streamwise 2mm length, spanwise 11mm width and vertical 0.4mm height. The total number of grid cells is about 2.88 million.

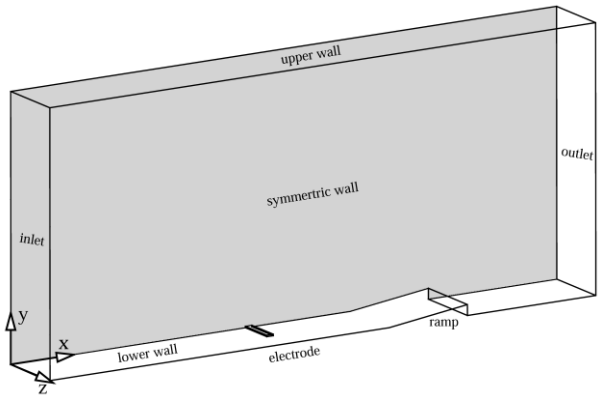

Fig.5 Computational Domain

4 Results and Discussion

4.1 Arc Discharge and Plasma Heating Model

A steady flow field is established after the wind tunnel runs for 4 seconds. The static pressure and Mach number in the test section reach 0.3bar and 2.47-2.48, respectively, as shown in Fig.6. The Mach number remains unchanged, while the static pressure decreases gradually with the wind tunnel running time. However, the discharge time is about 1s, during this duration the effect of the pressure decrease on the measurement is neglected.

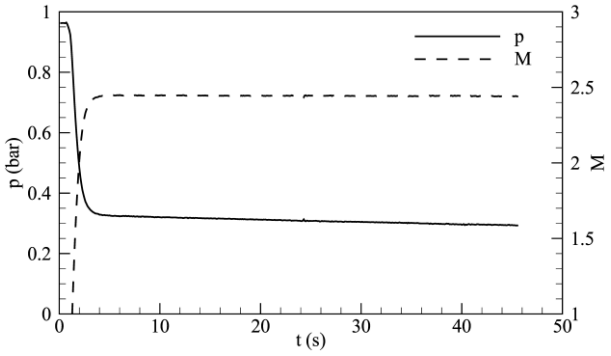

Fig.6 Static Pressure (p) and Mach Number (M)

4.1.1Effect of Power Supply on Arc Discharge

Two types of discharge are observed in different current outputs with same voltage of power supply. When the current limit of the power supply is set at 500mA, the transversal arc discharge is formed between the two adjacent electrodes as shown in Fig.7(a); The streamwise arc discharge is generated between the electrode and the compression ramp when the current limit increases to 800mA as shown in Fig.7(b). Fig.8(a) shows that the transversal discharge arc oscillates dramatically in voltage and current, which is consistent with the findings in reference [19], while the streamwise arc is more stable with the current fluctuation no more than 12% and voltage fluctuation not exceeding 19% as shown in Fig.8(b). The streamwise arc power is analyzed by the Discrete Fourier Transform (DFT) as shown in Fig.9. It can be seen that a steady heating process is dominant in the discharge which lays the foundation for the numerical model of plasma heating. In the subsequent experiments, only the streamwise discharge arc is generated.

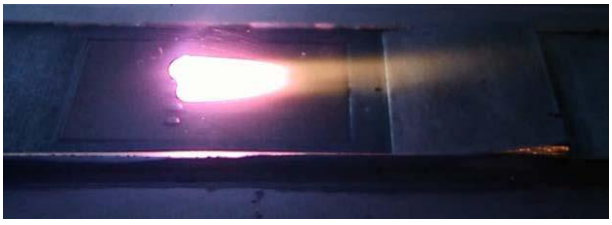

(a) Transversal Arc, (power supply: 8kV, 500mA)

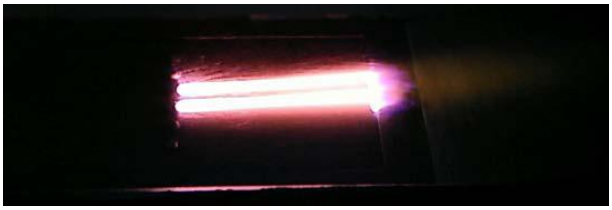

(b) Streamwise Arc, (power supply: 8kV, 800mA)

Fig.7 Discharge Arc

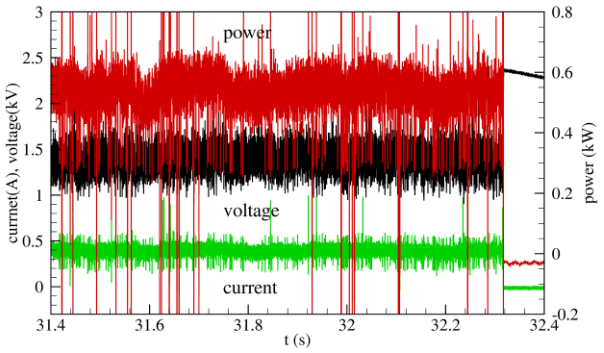

(a) Transversal Arc Parameter

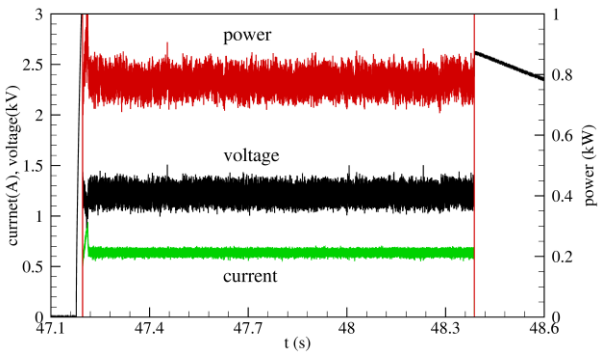

(b) Streamwise Arc Parameter

Fig.8 Discharge Arc Parameter

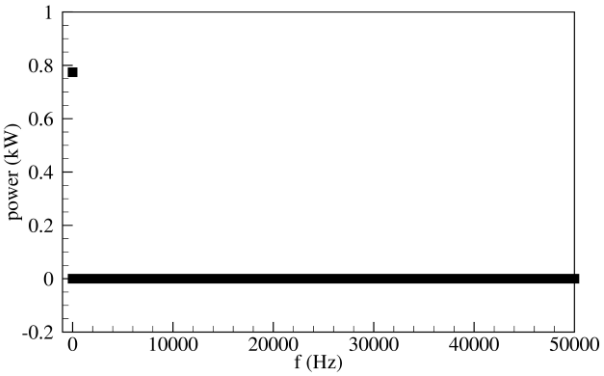

Fig.9 DFT for Streamwise Arc Power

4.1.2 Effect of Static Pressure on Arc Discharge

The limiting voltage and current are set at 8kV and 800mA to obtain the streamwise arc. The effect of static pressure on the discharge is studied. The variation of arc parameters with static pressure is recorded in Fig.10. It is shown that the arc voltage and power increase gradually with the increase of static pressure, while the arccurrent experiences a sudden decrease and remains constant even when the static pressure continues to increase. The reason for the current variation is still unknown. As the static pressure increases in the constant current region, both the electron mean free path (λ)

and the fraction of ionization (η) decrease [20] as shown in *Eqn.(4)* [21] and *Eqn.(5)* [22], respectively, leading to the reduction of electrical conductivity (σ) as seen in *Eqn.(6)* [23], which results the arc voltage and power increasing.

$$\lambda = \frac{RT}{\sqrt{2}\pi d^2 N_A \mathrm{p}} \tag{4}$$

$$\frac{\eta^2}{1-\eta^2}\cdot \mathrm{p} = \frac{2}{h^3}\frac{g_1}{g_0}(2\pi m)^{\frac{3}{2}}(k_B T)^{\frac{5}{2}}\exp(\frac{-\varepsilon}{k_B T}) \tag{5}$$

$$\sigma = \frac{ne^2\lambda}{mv_F} \tag{6}$$

Where λ is the electron mean free path, R is the molar gas constant, d is the molecular diameter, N_A is Avogadro's constant; η is the fraction of ionization, h is the Planck's constant, g_i is the degeneracy of states for the *i*-ions there only one level of ionization is considered, m is the electronic quality, k_B is Boltzmann's constant, ε is the ionization energy; σ is the electrical conductivity, n is the free electron number density, e is the electronic charge and v_F is the Fermi speed.

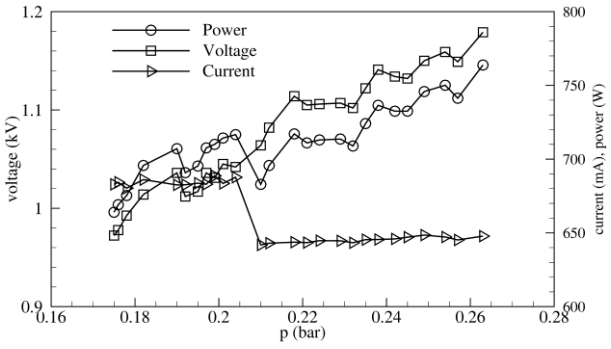

Fig.10 Arc Parameters VS Static Pressure

4.1.3 Plasma Heating Model

It is obtained the stable surface arc discharge as shown in Fig.11. The stable arc is modeled as an equivalent constant volume heating source based on plasma thermal effect and DFT analysis of the arc power as shown in Fig.12. The heating source in Fig.12(b) is a rectangular with streamwise 30mm length (73mm≤x≤103mm), spanwise 5mm width (0mm≤z≤5mm) and vertical 1.6mm height (0.4mm≤y≤2mm) based on the arc discharge figure (Fig.11). The spanwise width of the heating source is variable with the arc power. For arc power with 710W, the energy density of the heating source is

$$\rho_{\mathrm{power}} = \frac{\mathrm{P}}{\mathrm{V}} = \frac{710\mathrm{W}/2}{30\times 1.6\times 5\mathrm{mm}^3} = 1.48\times 10^9\ \mathrm{W/m^3} \tag{7}$$

Where ρ_{power} is the energy density, P is the equivalent arc power, V is the volume of heating source. It is assumed the heating source expands along spanwise and energy density keeps constant when the arc power increases, which will be validated in the next section.

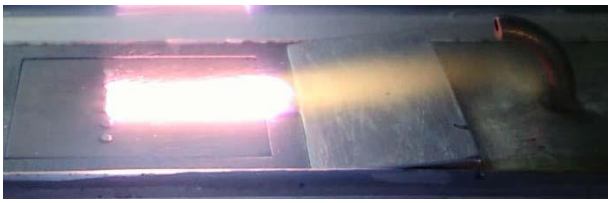

Fig.11 Stable Surface Arc Discharge

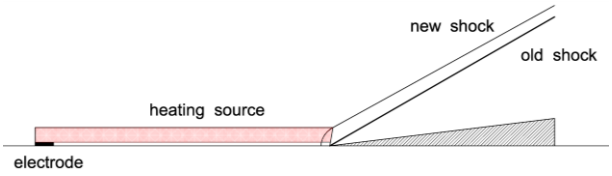

(a) Heating Source Schematic

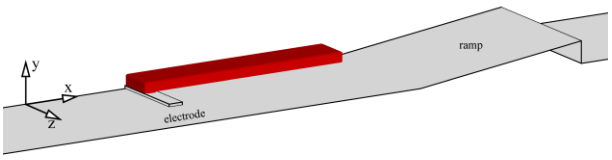

(b) Heating Source Location

Fig.12 Equivalent Volume Heating Source

4.2 Effect of Discharge on Oblique Shock

The effect of discharge on the oblique shock is analyzed by the pressure change and Schlieren images in the experiment along with the numerical simulation.

4.2.1 Pressure Change

First the discharge effect on the pressure at four specific locations (P1, P2, P3 and P4) for different arc powers is studied under the same static pressure in tunnel test section. Fig.13 presents the pressure change at four specific locations between discharge on and off. It can be seen that there is a significant rise of static

pressure right behind the arc region (point P2) because of the oblique shock shifting upstream induced by arc heating as the numerical result shown in Fig.14, which reveals the pressure variation in the centerline of lower wall with and without heating source, and a decrease of the pressure on the ramp surface (point P3) due to the weakening of original oblique shock. The static pressure upstream of the arc region (point P1) and the total pressure behind the shock (point P4) are almost kept unchanged. The pressure change of the four specific locations is insensitive to the discharge power. The surface pressure change is consistent with the numerical prediction as shown in Fig.15. What's more, increasing the heating source power from 710W to 852W with the same energy density, meanwhile the spanwise width of the heating source expands from 5mm to 6mm, the numerical result is still in good agreement with the experimental data. This indicates that the thermal effect of plasma plays an important role in the shock wave control and the numerically simplified heating model for the arc discharge is reasonable.

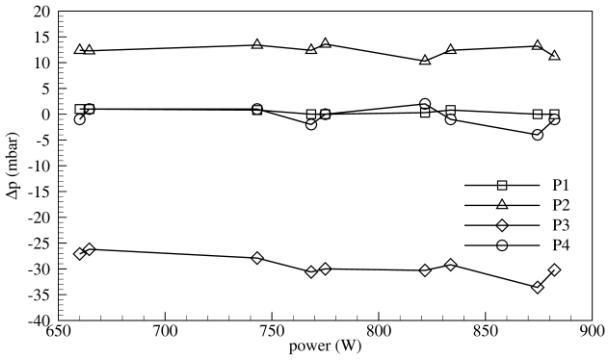

Fig.13 Pressure Change with Arc Power

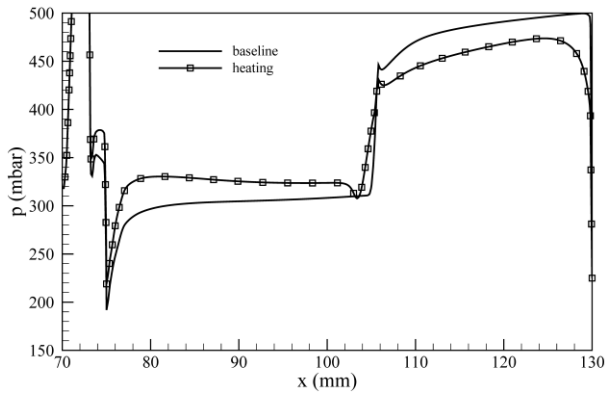

Fig.14 Pressure Change with Heating Source

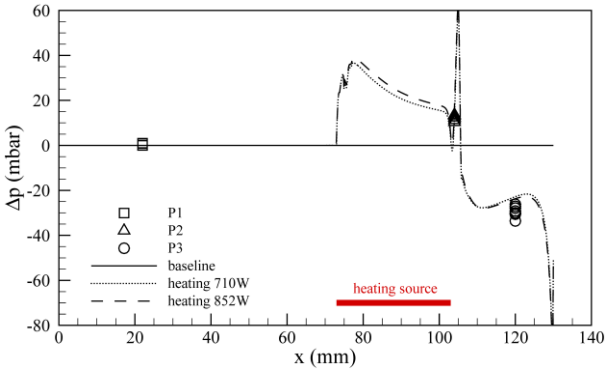

Fig.15 Pressure Change for Experiment and Simulation

Next, the effect of static pressure in the test section is studied while the arc power is kept in the range of 730-770W. As seen in Fig.16, the pressure change of point P1, P2 and P3 keep the same trend in different static pressure conditions respectively, while the total pressure at point P4 has more significant rise with arc discharge at low static pressure than high pressure conditions. This can be explained by the inviscid heated flow theory [24]. For supersonic flow, Mach number decreases ($dM < 0$) with heating ($dT_t > 0$) as shown in *Eqn.(8)*.

$$\frac{dM}{M} = \frac{(1+kM^2)[2+(k-1)M^2]}{4(1-M^2)} \frac{dT_t}{T_t} \qquad (8)$$

Therefore the Mach number in front of the original shock is smaller with discharge than that without it, leading to less total pressure loss for the arc heating condition. For the same incoming Mach number and temperature, as the static pressure in tunnel test section decreases, the mass flow rate decreases. For example, when the static pressure decreases from 0.3bar to 0.2bar, the mass flow rate will decrease from 1.374kg/s to 0.916kg/s. The decrease of mass flow rate induces larger change of T_t in the same power heating condition. The more increase of T_t, the more decrease of M based on *Eqn. (8)*. It can also be seen from Fig.17, there is a larger decline of Mach number at low static pressure than high one with same heating source. Therefore a smaller total pressure loss is expected at low static pressure.

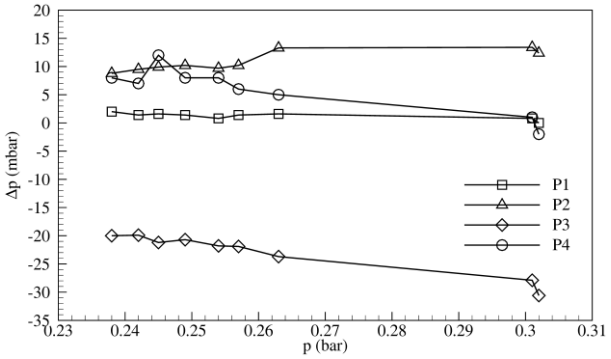

Fig.16 Pressure Change with Static Pressures

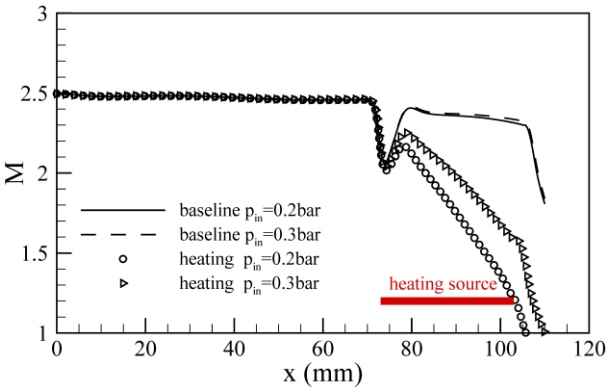

Fig.17 Mach Number Variation of y=2mm on Symmetry Plane

4.2.2 Shock Wave Change

The Schlieren images shown in Fig.18 suggest the arc discharge weaken oblique shock effectively. In the numerical work, with the heating source added, ramp shock weakens and shock angle increases significantly as shown in Fig.19, which is colored by the density streamwise change rate, which presents the shock structure just like Schlieren images observed in the experiments.

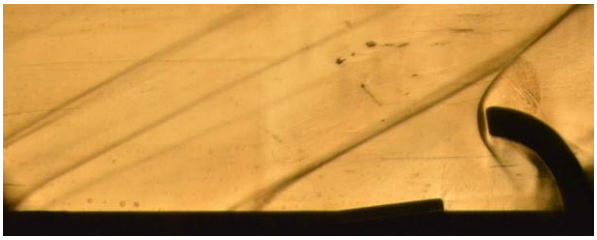

(a) Discharge off

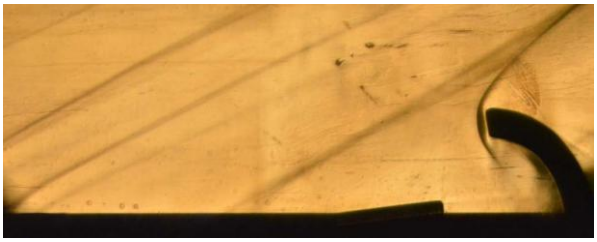

(b) Discharge on

Fig.18 Schlieren Images

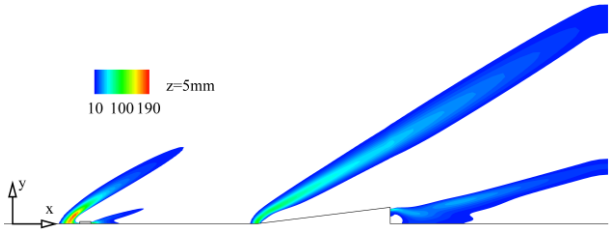

(a) No Heat Source

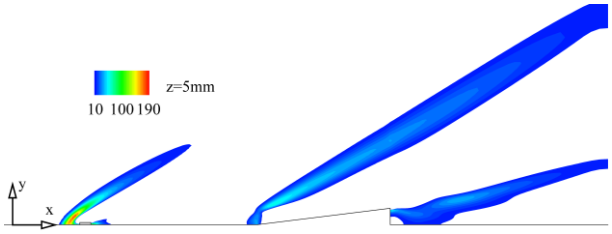

(b) With Heat Source

Fig.19 Density Streamwise Change Rate in Section of z=5mm

It has been found the discharge arc weaken ramp shock based on the pressure data and Schlieren images. The gas temperature and pressure increase instantly due to the arc heating, resulting in the increase of boundary layer thickness, the decrease of the Mach number and even a new shock wave generation with high discharge power input [18]. The thickening boundary layer acts like a soft wedge [16, 18], which leads to the ramp angle decrease and weakens the shock. The decrease of Mach number also reduces the shock strength. The new shock generated upstream of the discharge region reduces Mach number in the discharge region as well, which is expected to avoid in the study. This section will figure out the dominant role of the three factors based on the numerical results and measurement of shock angle through the Schlieren technique.

First, it is validated by numerical results that there is no new shock wave generated due to the arc heating with low power input in the experiments. In symmetry plane (z=0mm), the Mach number reduces obviously near the lower wall (y=2mm) around the heating source region, while there is no change of Mach number in y=5mm with heating source added as shown in Fig.20. There is either obvious decline of Mach number due to new shock generation in front of the heating source. It is concluded that there is no mew shock wave generated with low power

input in experiments and the Mach number reduces obviously due to the heating of source.

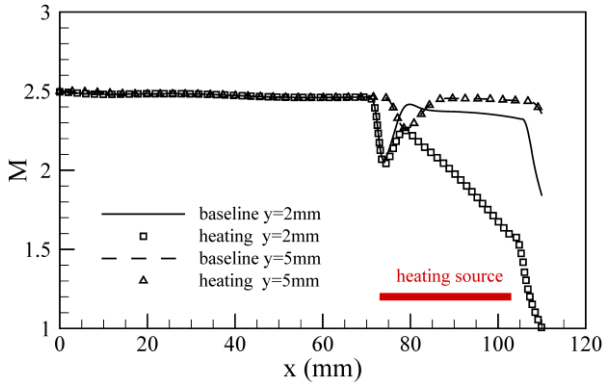

Fig.20 Mach Number Variation of y=2mm and 5mm on Symmetry Plane

Then the shock angle is measured in the Schlieren image as shown in Fig.21. Three streamwise coordinates (x_{pixel}) are selected and vertical coordinates (y_{pixel}) are determined by the maximum grayscale gradient as shown in Fig.22. There are two points with maximum grayscale gradient at one x_{pixel} coordinate because of the shock thickness. Finally the shock angle is calculated through linear regression of the six sampling points shown in Fig.23. It's shown that shock angle is increased by discharge arc. While arc heating weakens shock wave not only due to decreasing Mach number but also thickening boundary layer reducing the ramp angle [16,18]. The change of shock angle is based on the dominate one. According to the shock angle Formula as shown in *Eqn.(9)* [24],

$$\tan\delta = \frac{M^2\sin^2\beta - 1}{[M^2(\frac{k+1}{2} - \sin^2\beta) + 1]\tan\beta} \qquad (9)$$

Fig.24 reveals the variation of shock angle (β) with Mach number (M) and ramp angle (δ). It's found that the decrease of Mach number and ramp angle due to arc discharge induce shock angle changing oppositely. Under the experimental condition (M=2.5, δ = 7°), the change rate of β-M is much larger than β-δ. Since the decrease of Mach number due to the discharge arc heating is dominated in the shock angle change.

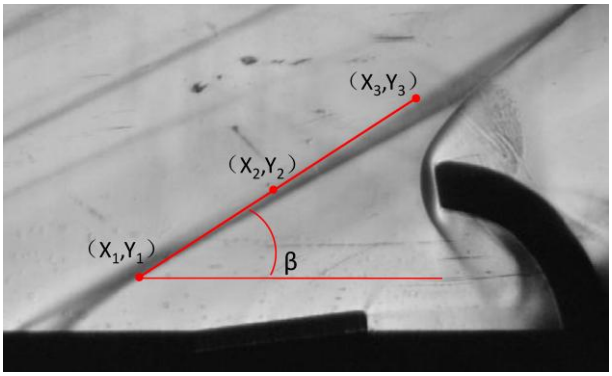

Fig.21 Shock Angle β

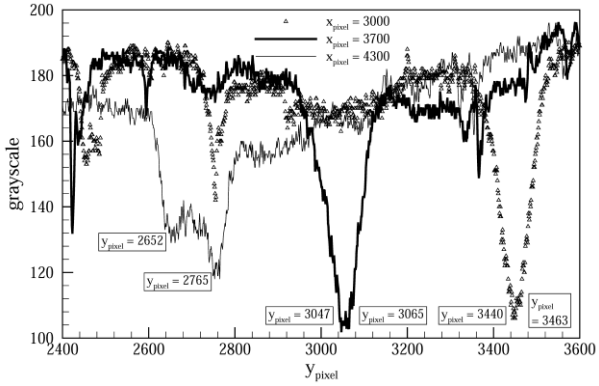

Fig.22 Grayscale Variation along y_{pixel} at Different x_{pixel}

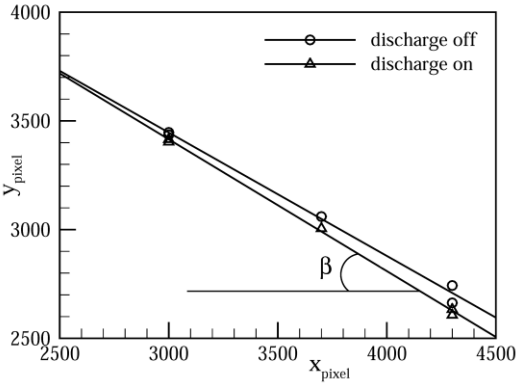

Fig.23 Linear Regression of Sampling Points

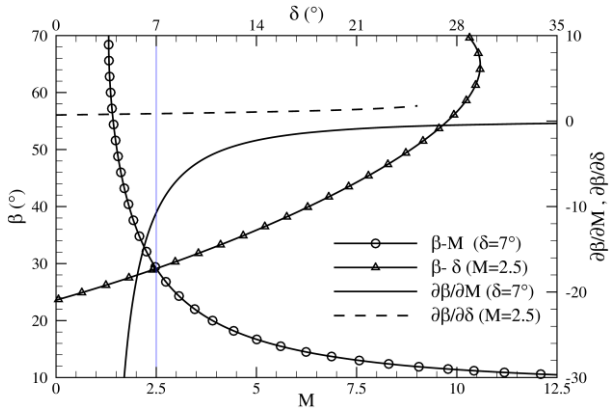

Fig.24 Shock Angle Change with Mach Number and Ramp Angle

4.2.3 Skin Friction and Total Pressure Change

In addition comparing skin friction coefficient (C_f) of the lower wall between baseline (without heating source) and heating case as shown in Fig.25, it's found that C_f has a significant decrease in the source region and downstream around the ramp. It also can be seen from the C_f variation in the symmetrical line of lower wall in Fig.26. That's because heating source leads to a high temperature region generated around the ramp and thickens the boundary layer as shown in Fig.27, which decreases the gradient of the local velocity leading C_f to decrease. The total pressure in the section of x=134mm, at which the point P4 is located as shown in Fig.4, has a significant rise in the region above the boundary layer and under the shock wave (5mm<y<20mm) as shown in Fig.28. The increase of total pressure behind the shock also indicates that heating source weakens the shock wave.

The two important parameters of supersonic inlet, C_f and total pressure recovery coefficient, are improved based on the numerical results with heating source model, which indicates that surface arc discharge plasma is a promising technique in shock wave control of supersonic inlet.

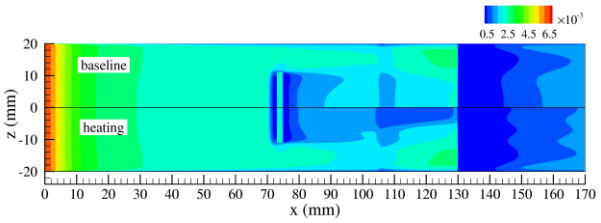

Fig.25 C_f of Lower Wall

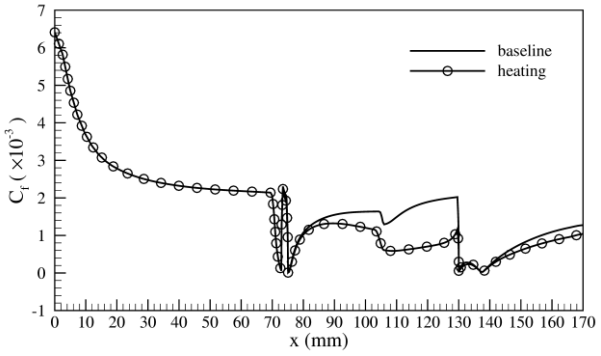

Fig.26 C_f in the Symmetrical Line of Lower Wall

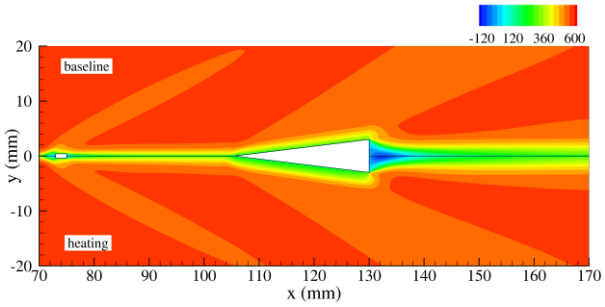

Fig.27 Heating Source Thickening Boundary Layer (Colored by streamwise velocity)

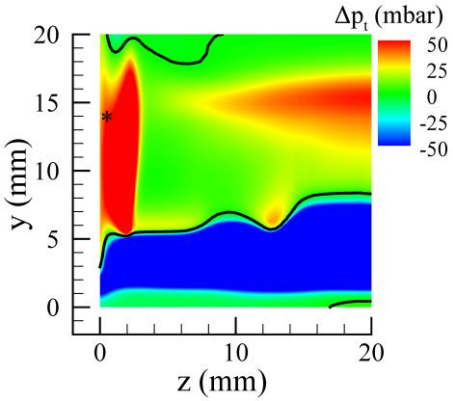

Fig.28 Total Pressure Change in Section of x=134mm

5 Conclusions

A combined numerical and experimental study of the effect of surface arc discharge plasma on oblique shock is performed. Two types of discharge are observed. One is generated between the two adjacent electrodes, forming an oscillating transversal arc, and the other is formed between the electrode and the compression ramp due to high power input, forming a stable streamwise arc. The experimental results show that the presence of the streamwise arc effectively reduces the oblique shock strength, leading to the increase of shock angle which is measured by Schlieren technique. The streamwise arc is modeled as an equivalent heating source based on the thermal effect of plasma in numerical simulation. Results show that the surface pressure increases in front of the oblique shock and decreases behind the shock, which is in good agreement with the experimental measurement. It also shows the significant advantage of arc discharge plasma in inducing shin friction and increasing total pressure recovery coefficient in supersonic inlet.

Acknowledgments

The project is sponsored by National Natural Science Foundation of China under grant No.51176157.

References

[1] Léger L, Moreau E, Artana G and Touchard G. (2001). Influence of a DC corona discharge on the airflow along an inclined flat plate. *Journal of Electrostatics*, *51*, 300-306.

[2] Roth J R, Sherman D M and Wilkinson S P (1998). Boundary layer flow control with a one atmosphere uniform glow discharge surface plasma, *AIAA paper*. 98-0328.

[3] Samimy M., Adamovich I, Webb B, Kastner J, Hileman J, Keshav S and Palm P. (2004). Development and characterization of plasma actuators for high-speed jet control. *Experiments in Fluids*, *37*(4), 577-588.

[4] Leonov S B, Firsov A A, Yarantsev D A, Falempin F and Goldfeld M. (2011). Plasma effect on shocks configuration in compression ramp. *AIAA paper*, *2362*.

[5] Cybyk B Z, Wilkerson J T and Grossman K R. (2004). Performance characteristics of the sparkjet flow control actuator. In *2nd AIAA Flow Control Conference* (Vol. 28).

[6] Moreau E. (2007). Airflow control by non-thermal plasma actuators. *Journal of Physics D: Applied Physics*, *40*(3), 605.

[7] Ustinov M V, Uspensky A A, Urusov A Yu and Rusianov D A. (2014). Laminar-turbulent transition control by dielectric barrier discharge, *Theory and Experiment. 29th Congress of the International Council of the Aeronautical Sciences*.

[8] Corke T C, Post M L and Orlov D M. (2009). Single dielectric barrier discharge plasma enhanced aerodynamics: physics, modeling and applications. *Experiments in Fluids*, *46*(1), 1-26.

[9] Samimy M., Kim J H., Kastner J, Adamovich I and Utkin Y. (2007). Active control of high-speed and high-Reynolds-number jets using plasma actuators. *Journal of Fluid Mechanics*, *578*, 305-330.

[10] Samimy M, Kearney-Fischer M and Kim J. H. (2012). High-speed and high Reynolds number jet control using localized arc filament plasma actuators. *Journal of Propulsion and Power*, *28*(2), 269-280.

[11] Firsov A A, Falempin F, Goldfeld M A and Leonov S B. (2013). Plasma control of shock wave configuration in M=2 inlet at off-design mode, *AIAA paper*, 2013-3115.

[12] Falempin F, Firsov A A, Yarantsev D A, Goldfeld M. A, Timofeev K and Leonov S B. (2015). Plasma control of shock wave configuration in off-design mode of M=2 inlet. *Experiments in Fluids*, *56*(3), 1-10.

[13] Li Ying-hong, Wu Yun, Song Hui-min, Liang Hua and Jia Min (2011). Plasma Flow Control, Aeronautics and Astronautics, Prof. Max Mulder (Ed.), ISBN: 978-953-307-473-3, InTech.

[14] Wang L, Luo Z, Xia Z., Liu B and Deng X. (2012). Review of actuators for high speed active flow control. *Science China Technological Sciences*, *55*(8), 2225-2240.

[15] Wang J, Li Ying-Hong, Cheng Bang-Qin, Sun Chang-Bing, Song Hui-Min and Wu Y. (2009). The mechanism investigation on shock wave controlled by plasma aerodynamic actuation. *ACTA PHYSICA SINICA*, Vol. 58, No. 8

[16] Leonov S, Soloviev V and Yarantsev D. (2006). High-speed inlet customization by surface electrical discharge. *AIAA Paper*, (2006-0403).

[17] Leonov S B and Yarantsev D. (2008). Near-surface electrical discharge in supersonic airflow: properties and flow control. *Journal of propulsion and power*, *24*(6), 1168-1181.

[18] Leonov S B, Firsov A A, Yarantsev D A, Falempin F and Miller A. (2010). Active steering of shock waves in compression ramp by nonuniform plasma. *Pulse*, *20*, 40.

[19] Leonov S B, Firsov A A, Yarantsev D A, Falempin F and Miller A. (2009). Flow control in model supersonic inlet by electrical discharge. *AIAA Paper*, *7367*.

[20] Carter R P and Murphree D L. (1969). Low-pressure arc discharge motion between concentric cylindrical electrodes in a transverse magnetic field. *AIAA Journal*, *7*(8), 1430-1437.

[21] *http://hyperphysics.phystr.gsu.edu/hbase/kinetic/menfre.html*

[22] *http://en.wikipedia.org/wiki/Saha ionization equation*

[23] *http://hyperphysics.phyastr.gsu.edu/hbase/electric/ohmmic.html*

[24] Wang Xin-Yue. *Fundamentals of aerodynamics*, Northwestern Polytechnical University, 1st edition, pp 154-157, pp 210-212.

Contact Author Email Address

Email: liufan1990@outlook.com

Copyright Statement